2

Indoor Channel Characterization and Performance Analysis of a 60 GHz near Gigabit System for WPAN Applications

Ghaïs El Zein, Gheorghe Zaharia,
Lahatra Rakotondrainibe and Yvan Kokar
European University of Brittany (UEB)
INSA, IETR, UMR 6164
20 Avenue des Buttes de Coësmes, CS 70839, 35708 Rennes Cedex 7
France

1. Introduction

During the last decade, substantial knowledge about the 60 GHz millimeter-wave (MMW) channel has been accumulated and different architectures have been analyzed to develop MMW communication systems for commercial applications. The 60 GHz bandwidth is suitable for high data-rate and short-distance wireless communications. This interest is particularly due to the large bandwidth and the important power loss caused by the free space and walls attenuation which permits to reuse the same frequency bandwidth even in the next floor of the same building. A high frequency band leads to a small size of RF components including antennas. However, many challenges have to be overcome before designing the system, such as the cost, millimeter-wave circuits and millimeter-wave propagation. For any wireless system design, the selection of a modulation and coding scheme is a main consideration and has a large impact on the system complexity. Problems such as power amplifier (PA) non-linearity, oscillator phase noise, insertion loss and flatness are more important for these RF circuits. These effects should be taken into account in the overall communication system. It was shown in (U. H. Rizvi et al., 2008) that single carrier (SC) transmission has a lower tolerance to phase noise and is more resistant to the PA non-linearity than the multicarrier OFDM. Owing to these advantages, in (S. Kato et al., 2009), the authors proposed the single carrier (SC) transmission for multi-gigabit 60 GHz WPAN systems, as defined in IEEE 802.15.3C standard. Recently, the IEEE 802.15.3c, ECMA and Very High Throughput (VHT) groups were formed to normalize the future WPAN systems for the 60 GHz band (ECMA, 2008). Hence, different architectures have been analyzed to develop new MMW communication systems for commercial applications. Up to now, in the literature, several studies have considered propagation measurements, potential applications, circuit design issues and several modulation techniques at 60 GHz (P. Smulders, 2002). However, few efforts have been dedicated to the realization of a 60 GHz wireless system and the characterization of its performance in realistic environments.

This chapter presents an overview of several studies concerning the indoor wireless communications at 60 GHz performed by the IETR (Institute of Electronics and Telecommunications of Rennes). This work is a part of research Techim@ges, CPER Palmyre II and IGCYC projects financially supported by Region Bretagne and UEB. The characterization and the modeling of the indoor radio propagation channel are based on several measurement campaigns obtained for different configurations. Some typical residential environments were also simulated by ray tracing and Gaussian Beam Tracking. The obtained simulations are compared to the experimental results. This chapter also presents a full experimental implementation of a 60 GHz wireless Gigabit Ethernet (G.E.) communication system operating at near gigabit data rate. As the 60 GHz radio link operates only in a single room configuration, a hybrid technology with the Radio-over-Fiber (RoF) is used to ensure the communications in all the rooms of a residential environment. The single carrier architecture chosen for this system is presented. In the baseband (BB) processing block, an original method used for the byte/frame synchronization is also described. The proposed system provides a good trade-off between performance and complexity. Performance measurements of the realized system for different configurations and different indoor environments are presented.
The rest of this chapter is organized as follows: Section 2 presents an overview of several studies realized at IETR concerning the measurements and characterization of the 60 GHz radio propagation channel. Section 3 reports recent work concerning a 60 GHz radio communication system. In Section 4, recent measurement and simulation results are presented. Conclusions and perspectives are drawn in Section 5.

2. Channel measurements and characterization

2.1 Channel sounder

During the last decade, several research activities were carried out at IETR in the 60 GHz bandwidth: the realization of the channel sounder, the indoor radio channel measurements, simulation and characterization. A 60-GHz wideband channel sounder was developed at IETR, as shown in Fig. 1. This channel sounder has 500 MHz bandwidth, 40 dB relative dynamic and 2.3 ns effective time resolution, which means that two paths separated from by 69 cm, can be correctly discriminated. Based on the sliding correlation technique, this sounder is optimized to perform long term measurement campaigns. Some measurement results with Doppler analysis up to 20 kHz are presented in (S. Guillouard et al., 1999).

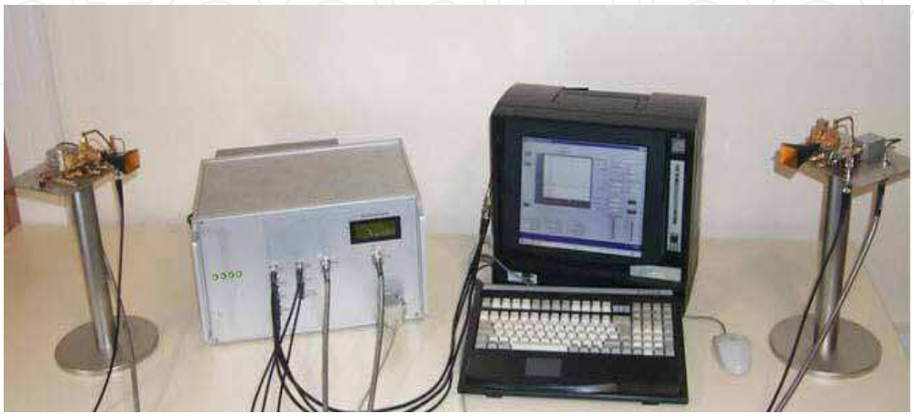

Fig. 1. Channel sounder at 60 GHz realized by IETR

2.2 Channel measurement and characterization

The study of wave propagation appears as an important task when developing a wireless system. The purpose of this chapter is to highlight different aspects concerning the wireless propagation channel at 60 GHz system (G. El Zein, 2009). In indoor environments, the radio propagation of electromagnetic waves between the transmitter (Tx) and the receiver (Rx), is characterized by the presence of multipath due to various phenomena such as reflection, refraction, scattering, and diffraction. In fact, the performance of communication systems is largely dependent on the propagation environment and on the structure of antennas. In this context, the space-time modeling of the channel is essential. For broadband systems, the analysis is usually made in the frequency domain and the time domain; this allows measuring the coherence bandwidth, the coherence time, the respective delay spread and Doppler spread values. Moreover, wave direction spread is used to highlight the link between propagation and system in the space domain. An accurate description of the spatial and temporal properties of the channel is necessary for the design of broadband systems and for the choice of the network topology. In (S. Collonge et al., 2004), the results of several studies concerning the radio propagation at 60 GHz in residential environments were published. These studies are based on several measurement campaigns realized with the IETR channel sounder (S. Guillouard et al., 1999). The measurements have been performed in residential furnished environments. The study of the angles-of-arrival (AoA) shows the importance of openings (such as doors, staircase, etc.) for the radio propagation between adjacent rooms (Fig. 2). In NLOS situation, the direct path is not available and the angular power distribution is more diffuse.

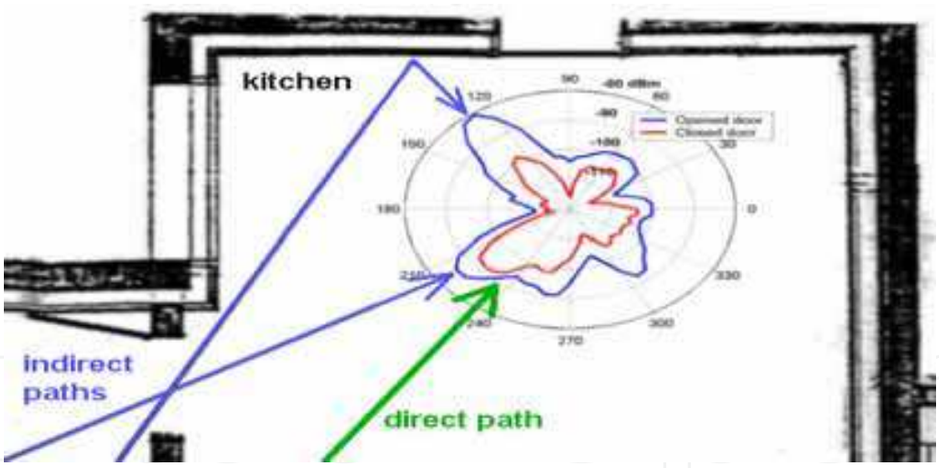

Fig. 2. Received power in the azimuthal plane (NLOS situation, with a horn antenna at Rx)

Radio propagation measurements between adjacent rooms show that the apertures (doors, windows, etc.) play a vital role in terms of power coverage. The wave propagation depends on antennas (beam-width, gain and polarization), physical environment (furniture, materials) and human activity. A particular attention is paid to the influence of the human activity on radio propagation, as shown in Fig. 3. The movements within the channel cause a severe shadowing effect; which can make the propagation channel not accessible during the shadowing event (S. Collonge et al., 2004). In this case, the angular diversity can be used; when a path is shadowed, another one, coming from another direction, can maintain the radio link.

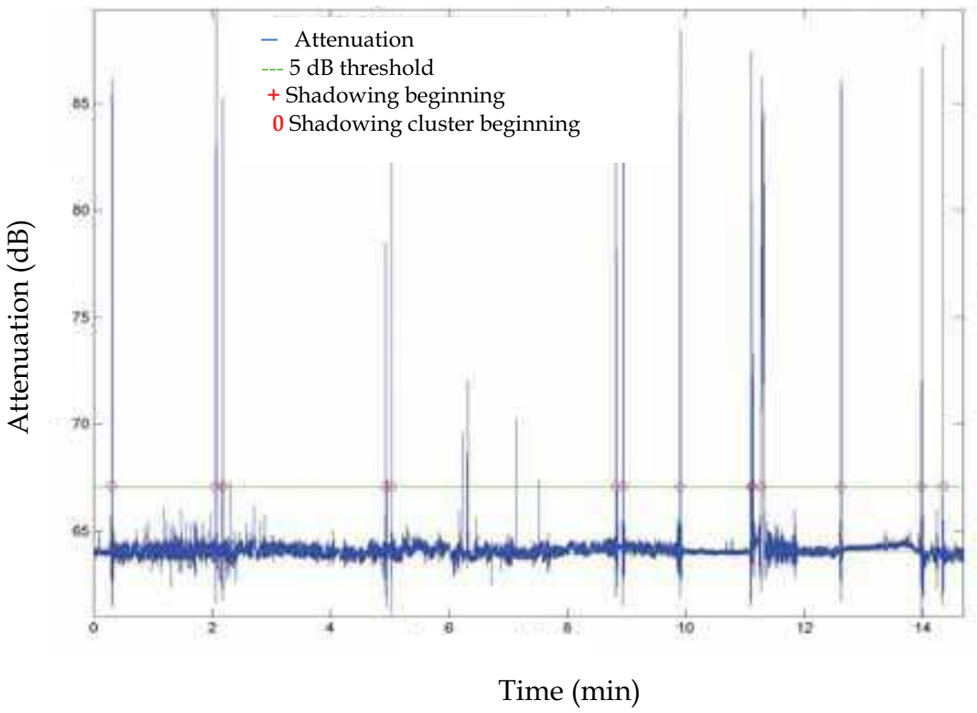

Fig. 3. Human activity measurement at 60 GHz (Rx antenna: horn, channel activity: 4 persons)

For the fading of the received signal, large-scale fading as well as small-scale effects are taken into consideration. Here, the large-scale fading at Tx-Rx distance, describes the average behavior of the channel, mainly caused by the free space path loss and the shadowing effect, while the small-scale fading characterizes the signal changes in a local area, only within a range of a few wavelengths (P. Smulders, 2009). From the database of impulse responses, several propagation characteristics are computed: attenuation, root mean square delay spread (τ_{RMS}), delay window, coherence bandwidth (B_{coh}) (S. Collonge et al., 2004). The use of directional antennas yield the benefits of reducing the number of multipath components (the channel frequency selectivity) and therefore to simplify the signal processing. Delay spread considerations reveal that RMS delay spread can be made very small (in the order of 1 ns when using narrow-beam antennas). This duration corresponds to the time symbol of 1 Gbps when using a simple BPSK modulation. Therefore, a data rate less than 1 Gbps can be achieved without further equalization. The coherence bandwidth $B_{coh,0.9}$ can be defined as the frequency shift where the correlation level falls below 0.9. As shown in (P. Smulders, 2009), the relationship between $B_{coh,0.9}$ and τ_{RMS} is obtained by:

$$B_{coh,0.9} = \frac{0.063}{\tau_{RMS}} \tag{1}$$

As shown in (N. Moraitis et al., 2004), when using directional antennas, the minimum observed coherence time was 32 ms (people walking at a speed of 1.7 m/s) which is much higher than the lower limit of 1 ms (omnidirectionnal antennas). The channel is considered

invariant during the coherence time. Therefore, it can be estimated once per few thousands of data symbols for Gbps transmission rate. The Doppler effect, due mainly to the moving persons in the channel, depends also on the antenna beamwidth. In indoor environments, when using directional antennas (spatial filtering), this Doppler effect is considered not critical.

2.3 Deterministic simulations tool of the 60 GHz radio channel

Deterministic models are based on a fine description of a specific environment. Two approaches can be identified: the site-specific ray tracing and the techniques based on the processing and exploitation of measured data. Based on optical approximations, ray-tracing models need to complete geometrical and electromagnetic specifications of the simulated environment. They enable to estimate the channel characteristics with a good accuracy, if the modelled environment is not too complex. The ray-tracing is generally based on a 3D description of the environment. A simplified model is a necessity, in order to reduce the simulation time and the computational resources. Requiring much computational time, other models can be used based on the Maxwell's equations.

As described in (R. Tahri et al., 2005), two deterministic simulation tools have been used to complement the experimental characterization: a ray-tracing tool and a 3 D Gaussian Beam Tracking (GBT) technique. The GBT method based on Gabor frame approach is particularly well suited to high frequencies and permits a collective treatment of rays which offers significant computation time efficiency. Fig. 4 shows the power coverage obtained with GBT and X-Siradif ray tracing software.

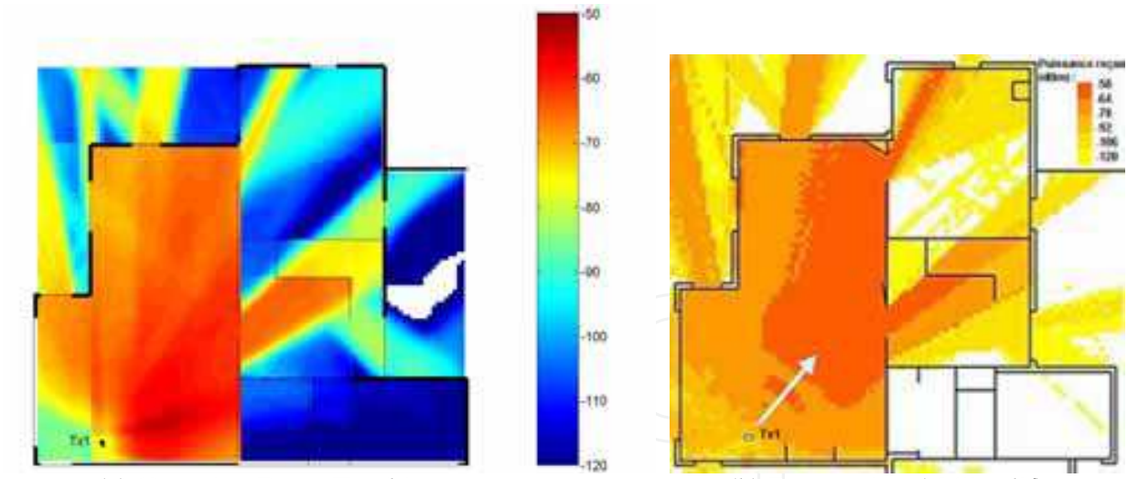

(a) Gaussian Beam Tracking (b) Ray tracing (X-Siradif)

Fig. 4. Power coverage map in the residential environment

The GBT algorithm and ray tracing technique are used for coverage simulations in an indoor environment (a house) at 60 GHz. The dimension of the house is 10.5×9.5×2.5 m^3. The building materials are mainly breeze blocks, plasterboards and bricks. The Tx (with patch antenna) is placed in a corner of the main room of the house, at a height of 2.2 m near the ceiling and slightly pointed toward the ground (15°). The azimuth angle is 50°. The receiving antenna (Rx) is a horn placed at a height of 1.2 m. At each location, the Rx antenna is pointing towards the Tx antenna. As one can observe in Fig. 4, the comparison of the

power distribution in the environment, obtained with GBT and X-Siradif, is very satisfying. More details are given in (S. Collonge et al., 2004).

3. System design

A 60 GHz wireless Gigabit Ethernet (G.E.) communication system operating at near gigabit throughput has been developed at IETR. The realized system is shown in Fig. 5.

Fig. 5. Wireless Gigabit Ethernet at 60 GHz realized by the IETR

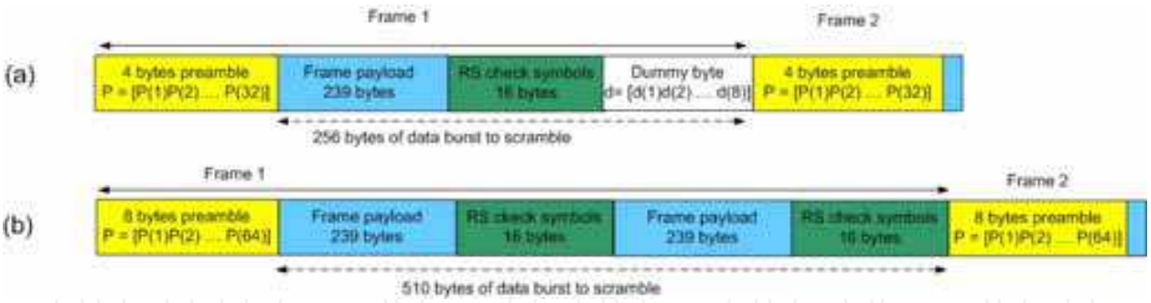

Fig. 6. Frame structure: a) 32-bits preamble; b) 64-bits preamble

This system covers 2 GHz available bandwidth. A differential binary shift keying (DBPSK) modulation and a differential demodulation are adopted at intermediate frequency (IF). In the baseband processing block, an original byte/frame synchronization technique is designed to provide a small value of the preamble false alarm and missing probabilities. Several measurements campaigns have been done for different configurations (LOS, NLOS, antenna depointing) and different environments (gym, hallways). In addition, bit error rate (BER) measurements have been performed for different configurations: with/without Reed Solomon RS (255, 239) coding and with byte/frame synchronization using 32/64 bits preambles. Our purpose is to compare the robustness of 32/64 bits preambles in terms of byte/frame synchronization at the receiver. The frame structure is shown in Fig. 6. The preambles are placed at the beginning of the frame payload of 239 bytes. As it will be shown

later, when using the 32-bits preamble, the frame/byte synchronization is not reliable. Therefore, a 64-bits preamble was considered. In order to avoid the reduction of the code rate, each 64-bits preamble is followed by 2 RS frames, as shown in Fig. 6. In this case, the frame length is Lf = 255*2+8 = 518 bytes.
The design and realization of the overall system including the baseband, intermediate frequency and radiofrequency blocks, are described in this section.

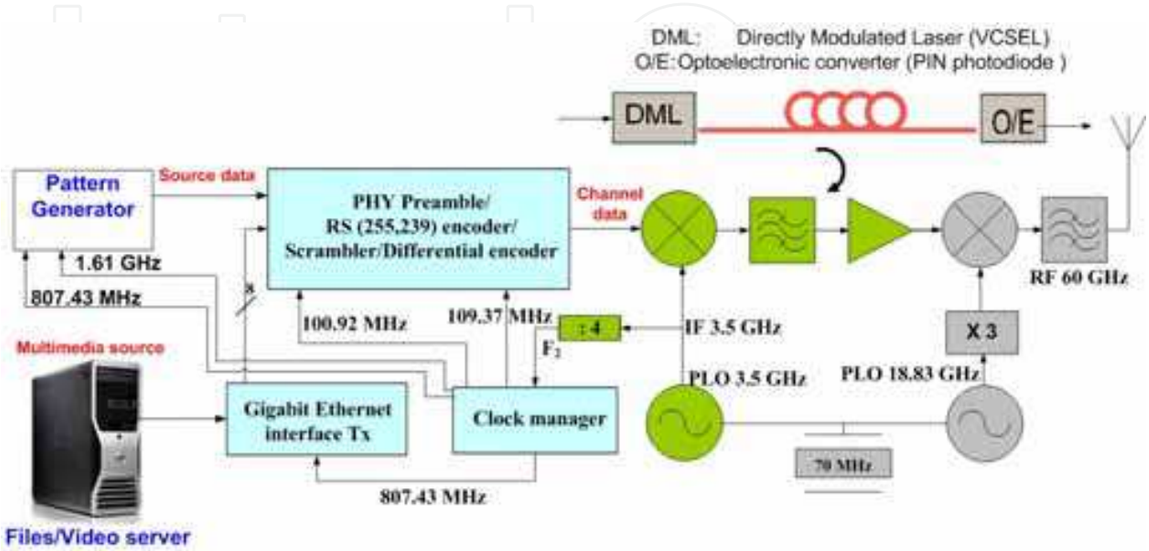

Fig. 7. 60 GHz wireless Gigabit Ethernet transmitter

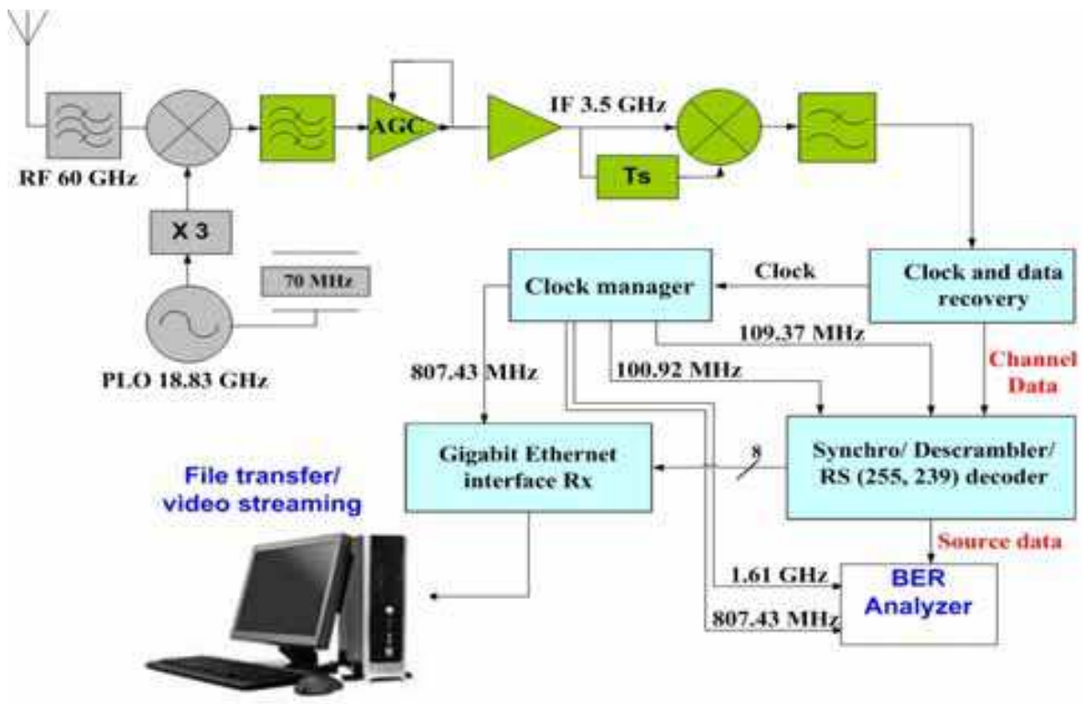

Fig. 8. 60 GHz wireless Gigabit Ethernet receiver

Fig. 7 and Fig. 8 show the block diagram of the Tx and Rx respectively. The realized system can operate with data received from a multimedia server using a G.E interface or from a pattern generator. As shown in Fig. 7, the clock of the encoded data is obtained from the intermediate frequency (IF = 3.5 GHz): F2 = IF/4 = 875 MHz. Using the frame structure with 64-bits preamble, the clock frequency for source data is:

$$f_1 = \frac{F_1}{8} = 100.929\,\text{MHz}, \qquad f_2 = \frac{F_2}{8} = 109.375\,\text{MHz}. \tag{2}$$

This frequency is obtained by the Clock manager block with a phase locked loop (PLL).
The transmitted signal must contain timing information that allows the clock recovery and the byte/frame synchronization at the receiver (Rx). Thus, scrambling and preamble must be considered. A differential encoder allows removing the phase ambiguity at the Rx (by a differential demodulator). Due to the hardware constraints, the first data rate was chosen at around 800 Mbps. Reed Solomon coding/decoding are used as a forward error correction.

3.1 Transmitter design

The G.E. interface of the transmitter is used to connect a home server to a wireless link with about 800 Mbps bit rate, as shown in Fig. 9.

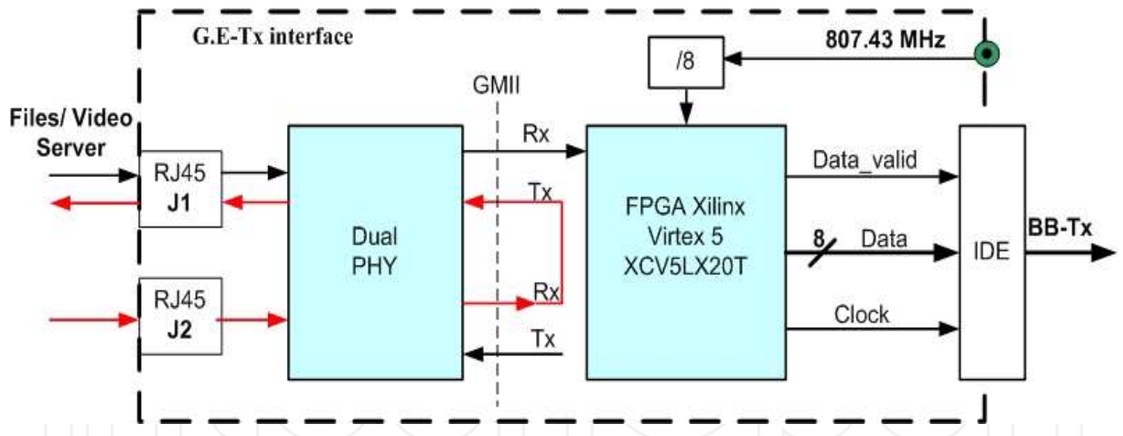

Fig. 9. Gigabit Ethernet interface of the transmitter

The gigabit media independent interface (GMII) is an interface between the media access control (MAC) device and the PHY layer. The GMII is an 8-bit parallel interface synchronized at a clock frequency of 125 MHz. However, this clock frequency is different from the source byte frequency f_1 = 807.43/8 =100.92 MHz generated by the clock manager in Fig. 7. Then, there is a risk of packet loss since the source is always faster than the destination. In order to avoid the packet loss, a programmable logic circuit (FPGA) is used. Therefore, the input byte stream is written into the dual port FIFO memory of the FPGA at a high frequency 125 MHz. The FIFO memory has been set up with two thresholds. When the upper threshold is attained, the dual PHY block (controlled by the

FPGA) sends a "stop signal" to the multimedia source in order to stop the byte transfer. Then, a frequency f_1 reads out continuously the data stored in the FIFO. In other hand, when the lower threshold is attained, the dual PHY block sends a "start signal" to begin a new Ethernet frame. Whatever the activity on the Ethernet access, the throughput at the output of the G.E. interface is constant. A header is inserted at the beginning of each Ethernet frame to locate the starting point of each received Ethernet frame at the receiver. Finally, the byte stream from the G.E. interface is transferred in the BB-Tx, as shown in Fig. 10.

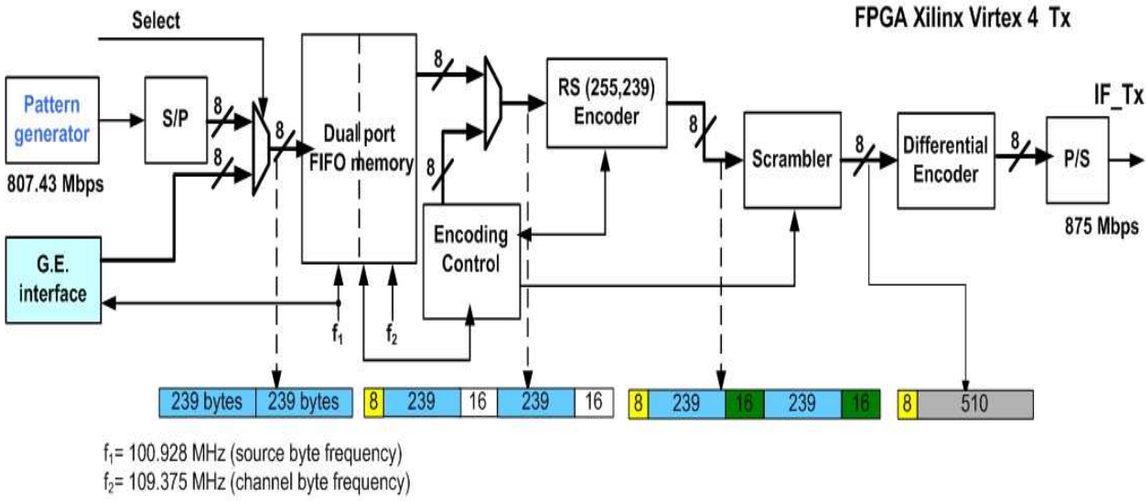

Fig. 10. Transmitter baseband architecture (BB-Tx)

A known pseudo-random sequence of 63 bits is completed with one more bit to obtain an 8 bytes preamble. This 8 bytes preamble is sent at the beginning of each frame to achieve good frame synchronization at the receiver. Due to the byte operation of a RS (255,239) coding, two clock frequencies f_1 and f_2 are used:

$$F_2 = \frac{3.5\,\text{GHz}}{4} = 875\,\text{MHz} \quad \text{and} \quad F_1 = \frac{2*239}{2*(239+16)+8} F_2. \tag{3}$$

The frame format is realized as follows: the input source byte stream is written into the dual port FIFO memory at a slow frequency f_1. When the FIFO memory is half-full, the encoding control reads out data stored in the register at a higher frequency f_2. The encoding control generates an 8 bytes preamble at the beginning of each frame, which is bypassed by the RS encoder and the scrambler. The RS encoder reads one byte every clock period. After 239 clock periods, the encoding control interrupts the bytes transfer during 16 clock periods, so 16 check bytes are added by the encoder. In all, two successive data words of 239 bytes are coded before creating a new frame. After coding, the obtained data are scrambled using an 8 bytes scrambling sequence. The scrambling sequence is chosen in order to provide at the

receiver the lowest false detection of the preamble from the scrambled data. Then, the obtained scrambled byte stream is differentially encoded before the modulation. The differential encoder performs the delayed modulo-2 addition of the input data bit (b_k) with the output bit (d_{k-1}):

$$d_k = b_k \oplus d_{k-1} \tag{4}$$

The obtained data are used to modulate an IF carrier generated by a 3.5 GHz phase locked oscillator (PLO) with a 70 MHz external reference. The IF signal is fed into a band-pass filter (BPF) with 2 GHz bandwidth and transmitted through a RoF link, as shown in Fig. 11. The RoF link consists of a laser diode, an optical variable attenuator, an optical fiber of length 300 meters and a photoreceiver. Then, this IF signal is used to modulate directly the current of a laser diode operating at 850 nm. At the receiver, the optical signal is converted to an electrical signal by a PIN diode and amplified.
The overall RoF link is designed to offer a gain of 0 dB. The IF signal is sent to the RF block. This block is composed of a mixer, a frequency tripler, a PLO at 18.83 GHz and a band-pass filter (59-61 GHz). The local oscillator frequency is obtained using an 18.83 GHz PLO with the same 70 MHz reference and a frequency tripler. The phase noise of the 18.83 GHz PLO signal is about –110 dBc/Hz at 10 kHz off carrier. The BPF prevents the spill-over into adjacent channels and removes out-of-band spurious signals caused by the modulator operation. The 0 dBm obtained signal is fed into the horn antenna with a gain of 22.4 dBi and a half power beamwidth (HPBW) of 10°V and 12°H.

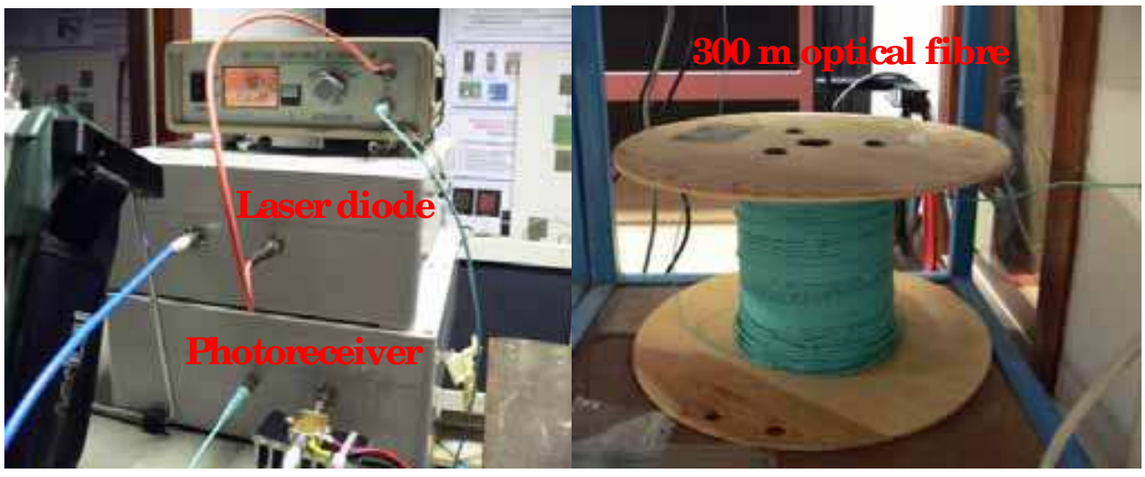

Fig. 11. Radio over Fibre link

3.2 Receiver design

The receive antenna, identical to the transmit horn antenna, is connected to a band-pass filter (59-61 GHz). The RF filtered signal is down-converted to an IF signal centered at 3.5 GHz and fed into a band-pass filter with a bandwidth of 2 GHz. An automatic gain control (AGC) with 20 dB dynamic ranges is used to ensure a quasi-constant signal level at the demodulator input when, for example, the Tx-Rx distance varies. The AGC loop consists of

a variable gain amplifier, a power detector and a circuitry using a baseband amplifier to deliver the AGC voltage. This voltage is proportional to the power of the received signal. A low noise amplifier (LNA) with a gain of 40 dB is used to achieve sufficient gain. A simple differential demodulation enables the coded signal to be demodulated and decoded. In fact, the demodulation, based on a mixer and a delay line (delay equal to the symbol duration Ts = 1.14 ns), compares the signal phase of two consecutive symbols. A "1" is represented as a π-phase change and a "0" as no change. Owing to the product of two consecutive symbols, the ratio between the main lobe and the side lobes of the channel impulse response increases. This means that the differential demodulation is more resistant to intersymbol interference (ISI) effect compared to a coherent demodulation. Nevertheless, this differential demodulation is less performing in additive white Gaussian noise (AWGN) channel. Following the loop, a low-pass filter (LPF) with 1.8 GHz cut-off frequency removes the high frequency components of the obtained signal. For a reliable clock acquisition realized by the clock and data recovery (CDR) circuit, long sequences of '0' or '1' must be avoided. Thus, the use of a scrambler (and descrambler) is necessary.
A block diagram of the baseband architecture of the receiver is shown in Fig. 12. Owing to the RS (255, 239) decoder, the synchronized data from the CDR output are converted into a byte stream.

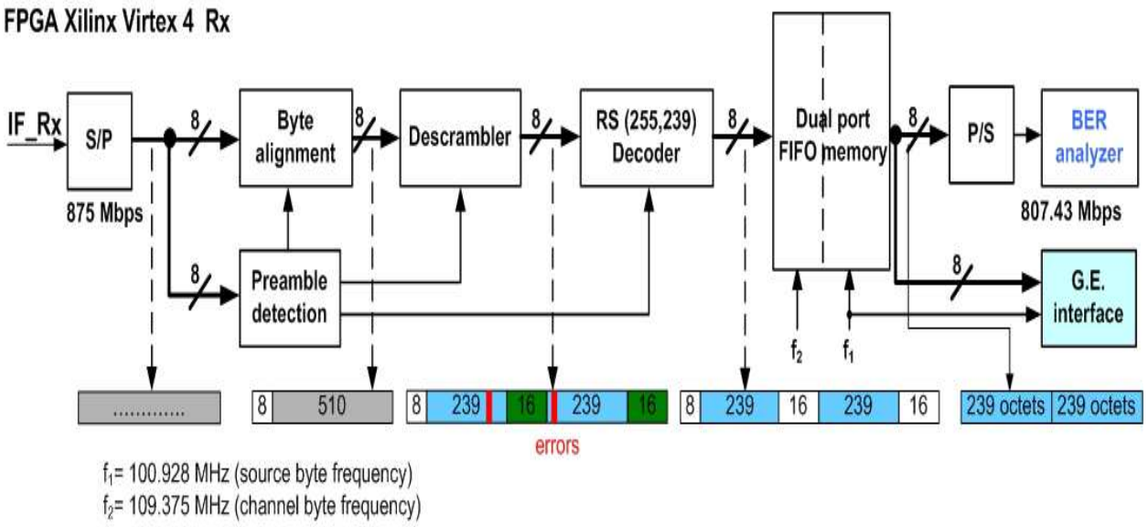

Fig. 12. Receiver baseband architecture (BB-Rx)

Fig. 13 shows the architecture of byte/frame synchronization using a 64 bits preamble.
The preamble detection is based on the cross-correlation of 64 successive received bits and the internal 64 bits preamble. Further, each C_k ($1 \le k \le 8$) correlator of 64 bits must analyze a 1-bit shifted sequence. Therefore, the preamble detection is performed with 64+7 = 71 bits, due to the different possible shifts of a byte. In all, there are 8 correlators in each bank of correlators. In addition, in order to improve the frame synchronization performance, two banks of correlators are used, taking into consideration the periodical repetition of the preamble: P1 (8 bytes) + D1 (510 bytes) + P2 (8 bytes) + D2 (510 bytes) + P3 (8 bytes). This

process diminishes the false alarm probability (Pf) while the missing detection probability (Pm) is approximately multiplied by 2, as shown later. The preamble detection is obtained if the same C_k correlators in each bank of correlators indicate its presence. Therefore, the decision is made from 526 successive bytes (P1 + D1 + P2) of received data stored by the receiving shift register. In fact, the value of each correlation is compared to a threshold (S) to be determined. Setting the threshold at the maximum value (S = 64) is not practical, since a bit error in the preamble due to the channel impairments leads to a frame loss. A trade-off between Pm and Pf gives the threshold to be used. A false alarm is declared when the same C_k correlators in each bank of correlators detect the presence of the preamble within the scrambled data (D1 and D2).

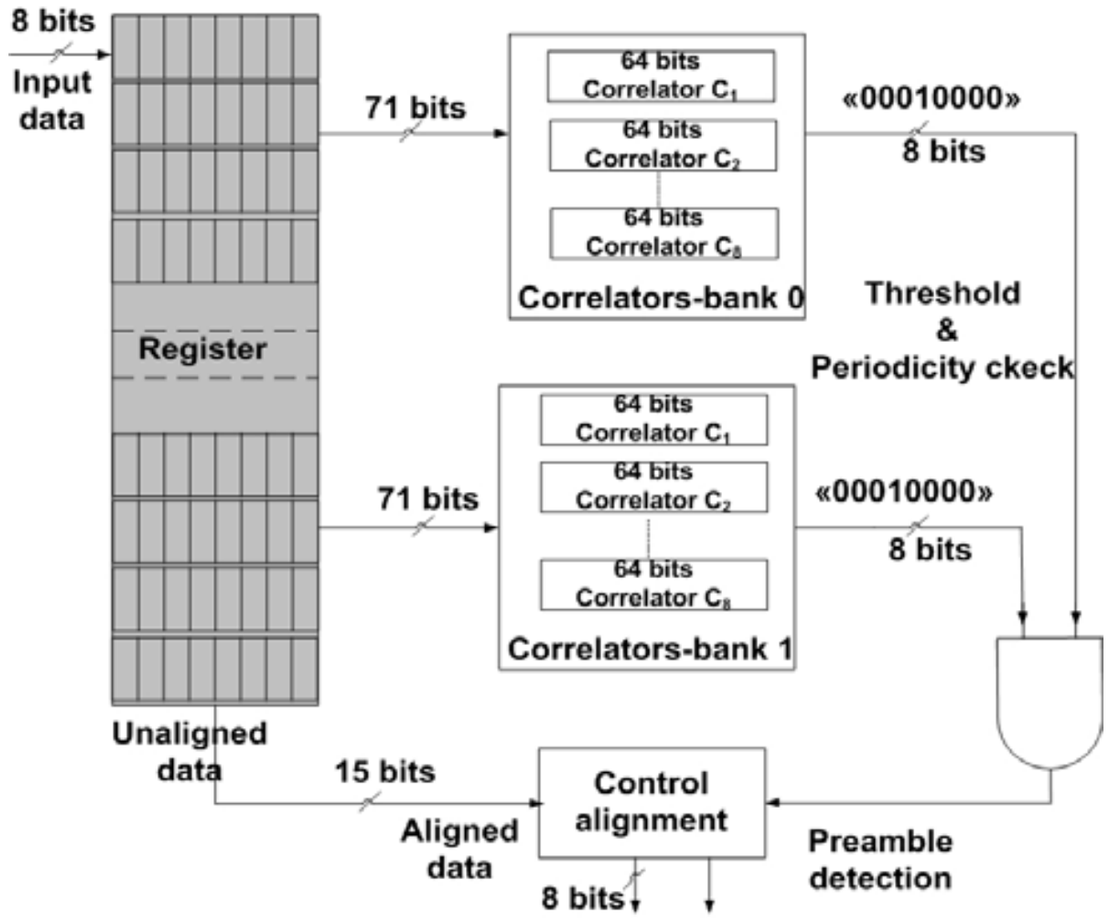

Fig. 13. The preamble detection and byte synchronization

The frame acquisition performance of the proposed 64 bits preamble was evaluated by simulations and compared to that of the 32 bits preamble (L. Rakotondrainibe et al., 2009). The frame structure with 32 bits preamble uses only a data word of 256 bytes (255 bytes + a "dummy byte"). Fig. 14a and Fig. 14b show the missing probability (Pm) versus channel error probability (p) for an AWGN channel, with 32 and 64 bits preamble, respectively. P_{m1} and P_{m2} are the missing detection probability using one bank and two banks of correlators, respectively.

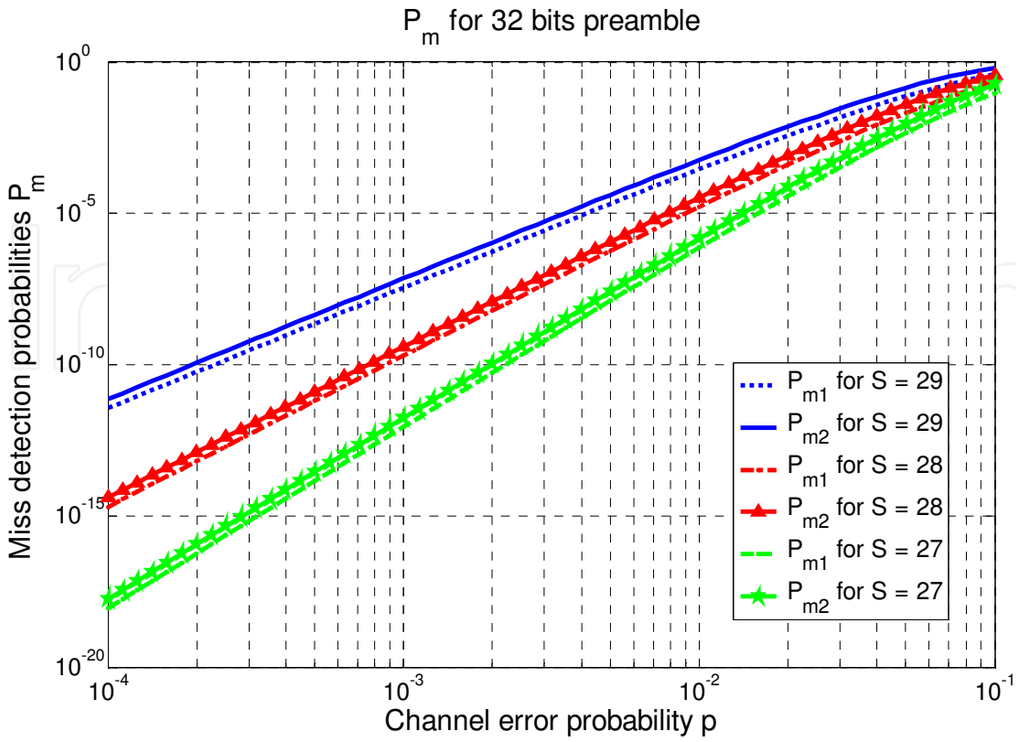

Fig. 14a. Miss detection probability with 32 bits preamble

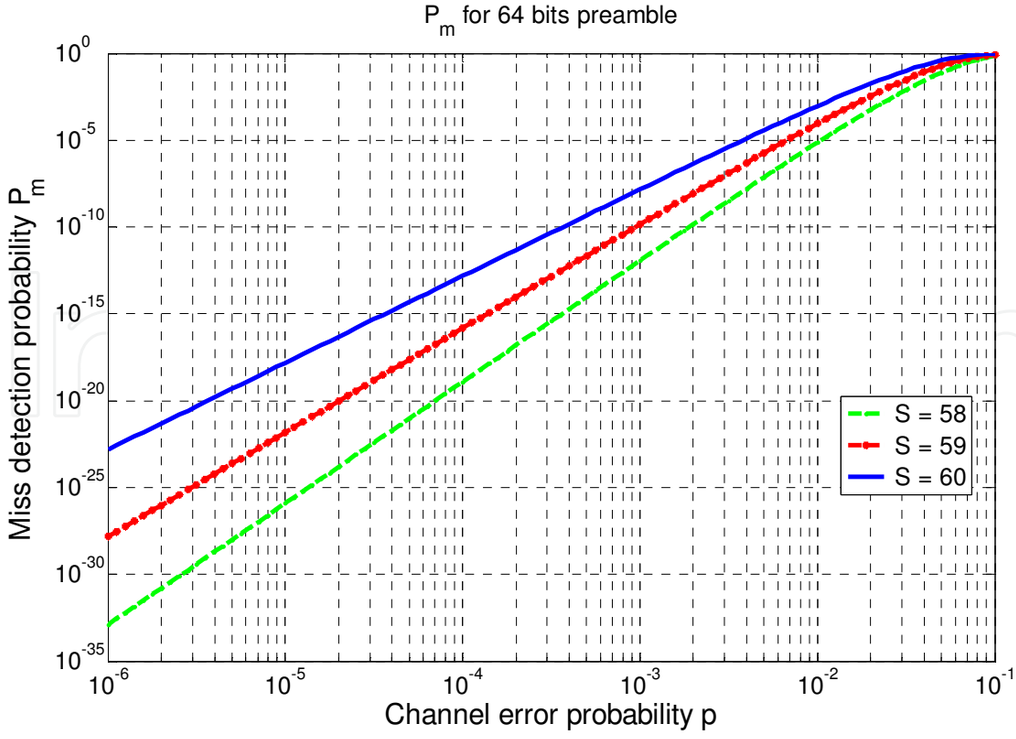

Fig. 14b. Miss detection probability with 64 bits preamble

Fig. 15a and Fig. 15b show the false alarm probability versus threshold S, with 32 and 64 bits preamble, respectively.

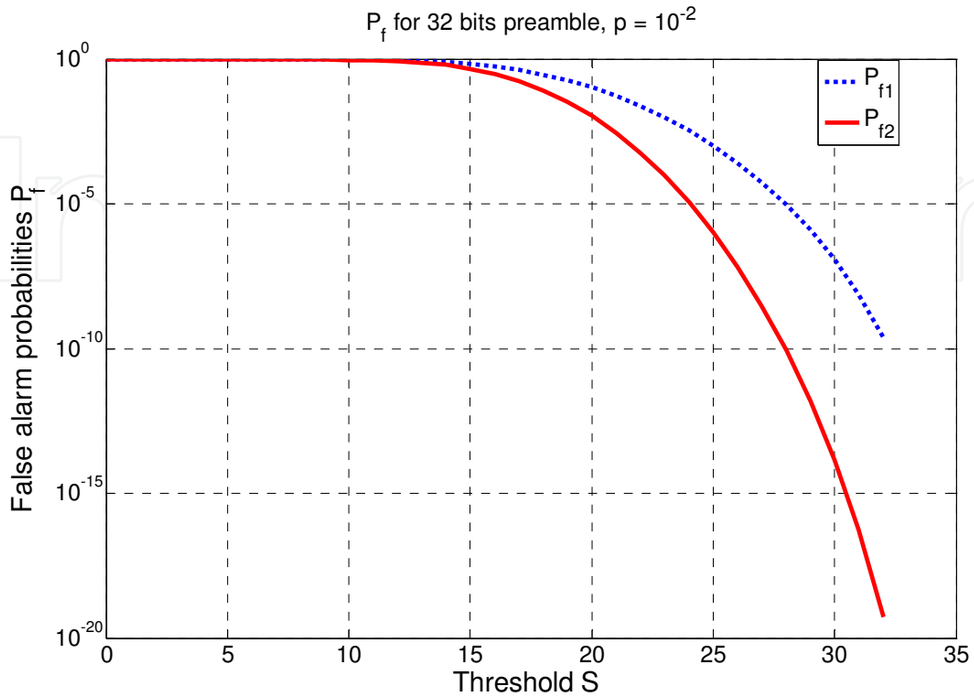

Fig. 15a. False alarm probability with 32 bits preamble

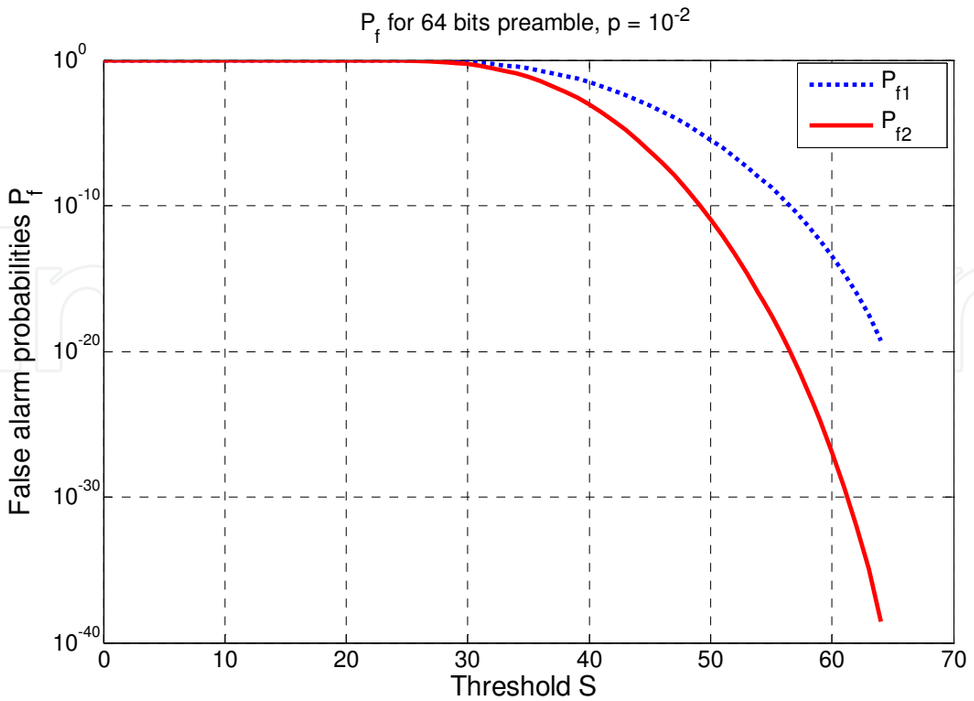

Fig. 15b. False alarm probability with 64 bits preamble

In these figures, P_{f1} and P_{f2} indicate the false alarm probabilities using one and two banks of correlators, respectively. The effect of p on the false alarm probability is insignificant since the random data bits "0" and "1" are assumed to be equiprobable. With the 64 bits preamble, for p = 10^{-3}, the result indicate that $P_m = 10^{-10}$ and $P_{f2} = 10^{-24}$ for S = 59. However, with the 32 bits preamble, we obtain $P_m = 10^{-7}$, $P_{f2} = 10^{-13}$ for S = 29. This means that, for a data rate about 1 Gbps, the preamble can be lost several times per second because $P_m = 10^{-7}$ (S = 29) with 32 bits preamble. We can notice that, for given values of p and P_{F2}, the 64 bits preamble shows a smaller false alarm probability compared to that obtained with the 32 bits preamble.
After the synchronization, the descrambler performs the modulo-2 addition between 8 successive received bytes and the descrambling sequence of 8 bytes. At the receiver, the baseband processing block regenerates the transmitted byte stream, which is then decoded by the RS decoder. The RS (255, 239) decoder can correct up to 8 erroneous bytes and operates at a fast clock frequency f_2 = 109.37 MHz. The byte stream is written discontinuously into the dual port FIFO memory at a fast clock frequency f_2. A slow clock frequency f_1 = 100.92 MHz reads out continuously the byte stream stored by the register, since all redundant information is removed. Afterwards, the byte stream is transferred to the receiver Gigabit Ethernet interface, as shown in Fig. 16. The feedback signal can be transmitted via a wired Ethernet connection or a Wi-Fi radio link due to its low throughput.

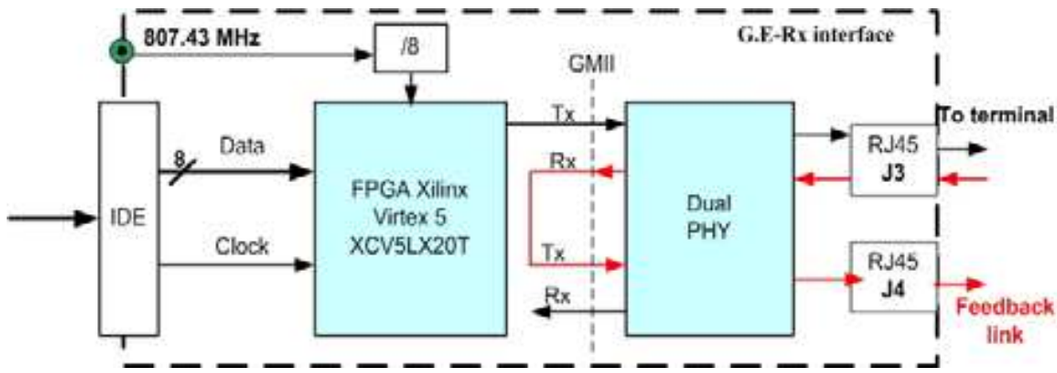

Fig. 16. Receiver Gigabit Ethernet interface

4. System performance analysis

4.1 System bandwidth

A vector network analyzer (HP 8753D) is used to measure the frequency response and impulse response figures of RF blocks including the LOS propagation channel by the parameter S_{21}. The objective was to determine the system bandwidth and to estimate the multipath channel effects, when using directional horn antennas. Measurements were performed in a corridor where the major part of the transmitted power is focused in the direction of the receiver. The RF-Tx and RF-Rx were placed at a height of 1.5 m. After measurement set-up and calibration, we obtain 2 GHz available bandwidth from the frequency response figure (Fig. 17). However, the RF blocks present some ripples in the band of flatness around 2 dB.
A perfect system must have an impulse response with only one lobe. Fig. 18 presents the result of an impulse response of the RF Tx-Rx blocks at 10 m Tx-Rx distance. A back-to-back test was realized using a 45 dB fixed attenuator at 60 GHz but similar results were obtained. Therefore, few side lobes were obtained which are mainly due to RF components imperfections.

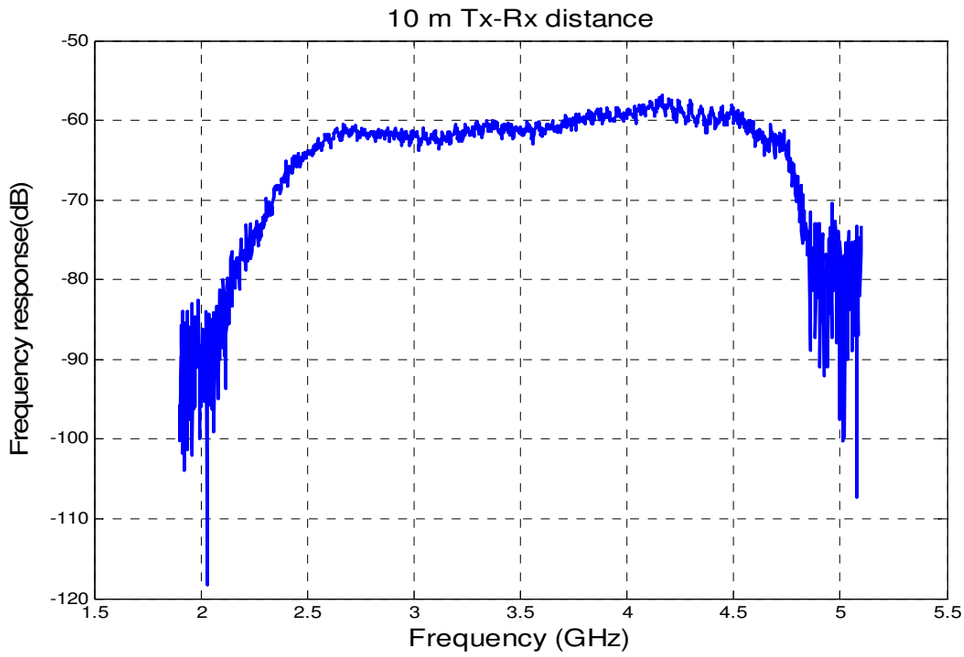

Fig. 17. Frequency response of RF blocks (Tx & Rx) using horn antennas

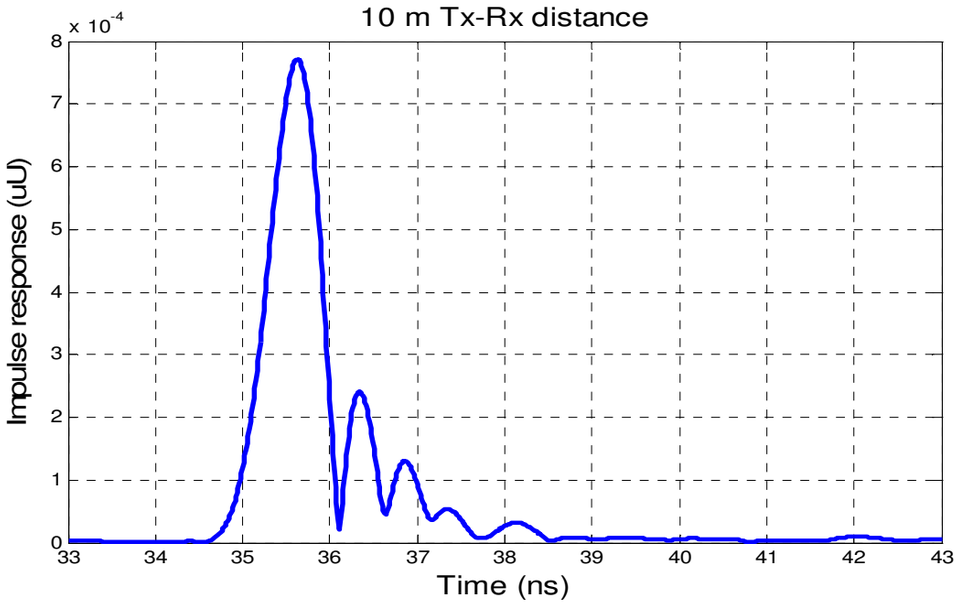

Fig. 18. Impulse response of RF blocks (Tx & Rx) using horn antennas

4.2 IF back-to-back performance results

The objective is to determine the signal to noise ratio (SNR) degradation of the realized DBPSK system with an ideal DBPSK system at a same bit error rate (BER).

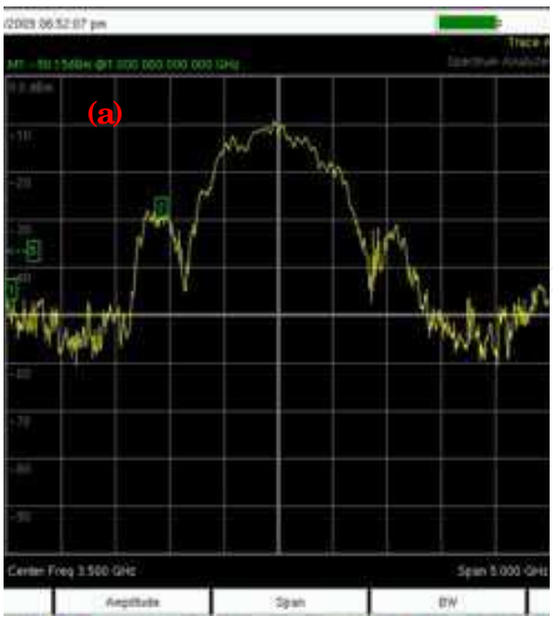

Fig. 19a. IF-Rx spectrum without noise

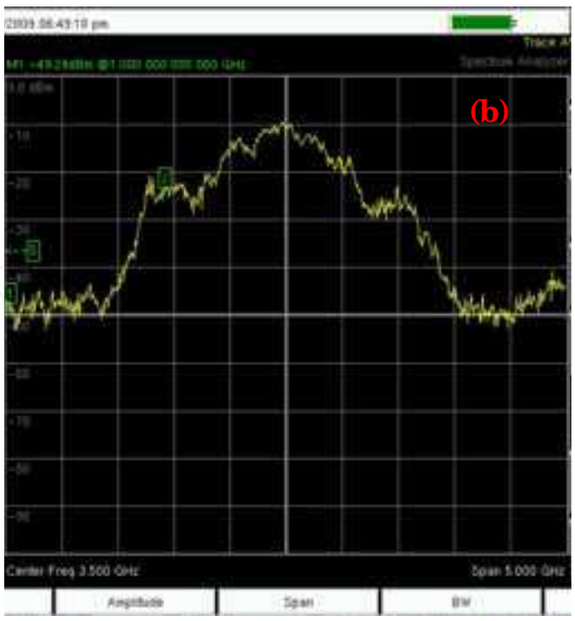

Fig. 19b. IF-Rx spectrum with noise

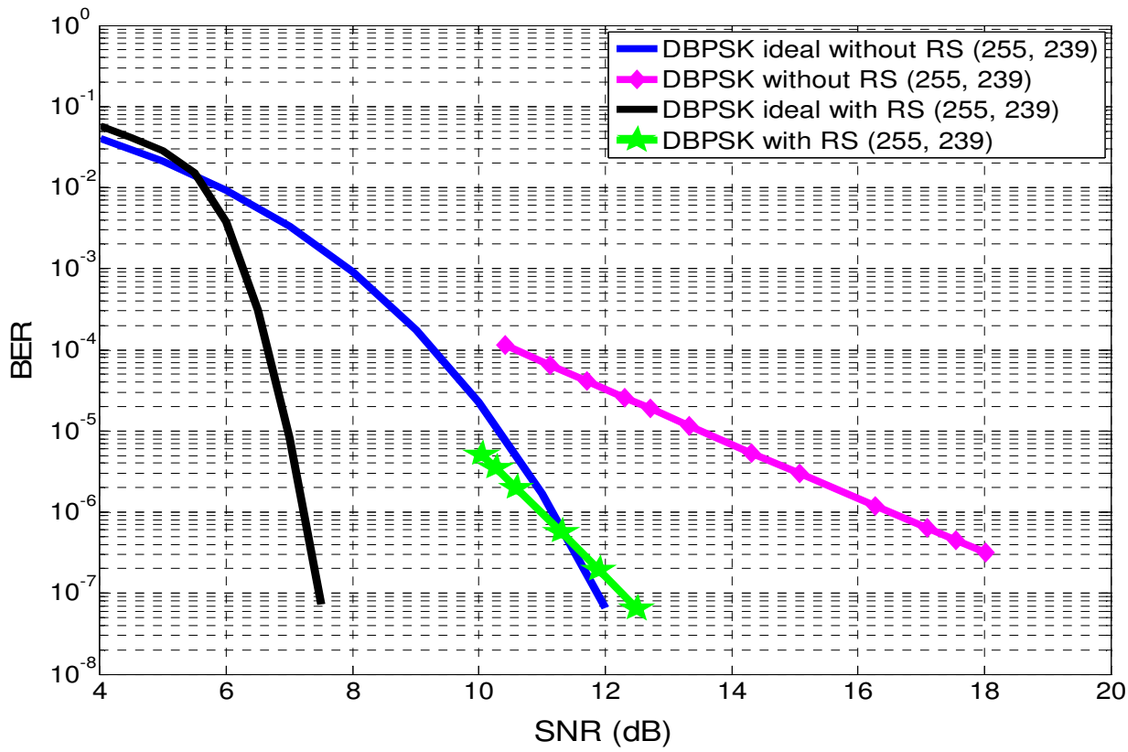

Fig. 20. BER versus SNR in the presence of AWGN

Back-to-back test of the realized DBPSK system (without RF blocks and AGC loop) was carried out at IF. The goal is to evaluate the BER versus SNR at the demodulator input. Hence, an external AWGN is added to the IF modulated signal (before the IF-Rx band pass

filter). The external AWGN is a thermal noise generated and amplified by successive amplifiers. This noise feeds a band pass filter and a variable attenuator so that the SNR is varied by changing the noise power. Fig. 19a and Fig. 19b show the spectrum at IF, without and with extra AWGN respectively. The measured BER versus SNR is shown in Fig. 20. Compared to an ideal system, at a BER of 10^{-5}, the SNR degradation of the realized system is about 3.5 and 3 dB for uncoded and coded data, respectively. Indeed, at the receiver, the 2 GHz bandwidth of the filter is too wide for a throughput of 875 Mbps. In order to avoid the increased power noise in the band, the filter bandwidth could be reduced to 1.1 GHz, for example.

4.3 Link budget

Using the free space model, Fig. 21 shows the estimated IF received power versus the Tx-Rx distance. This result takes into account the 0 dBm transmitted power, the antenna gains (horn or patch), the path loss (free space model) and the implementation losses of RF blocks. Two types of antennas were used: horn antenna and patch antenna. The patch antenna has a gain of 8 dBi and a HPBW of 30°. The IF receiver noise power is:

$$N_L = -174\,(\mathrm{dBm}/\mathrm{Hz}) + \mathrm{NF} + 10\log(B) = -71.98\,\mathrm{dBm}. \quad (5)$$

where NF = 9 dB is the total noise figure and B = $2*10^9$ Hz is the receiver bandwidth. As shown in Fig. 20, the minimum SNR needed for BER = 10^{-4} is about 10.5 dB. Thus, the receiver sensitivity is about P_S = - 61.5 dBm. Therefore, the demodulator input power must be greater than 0 dBm.

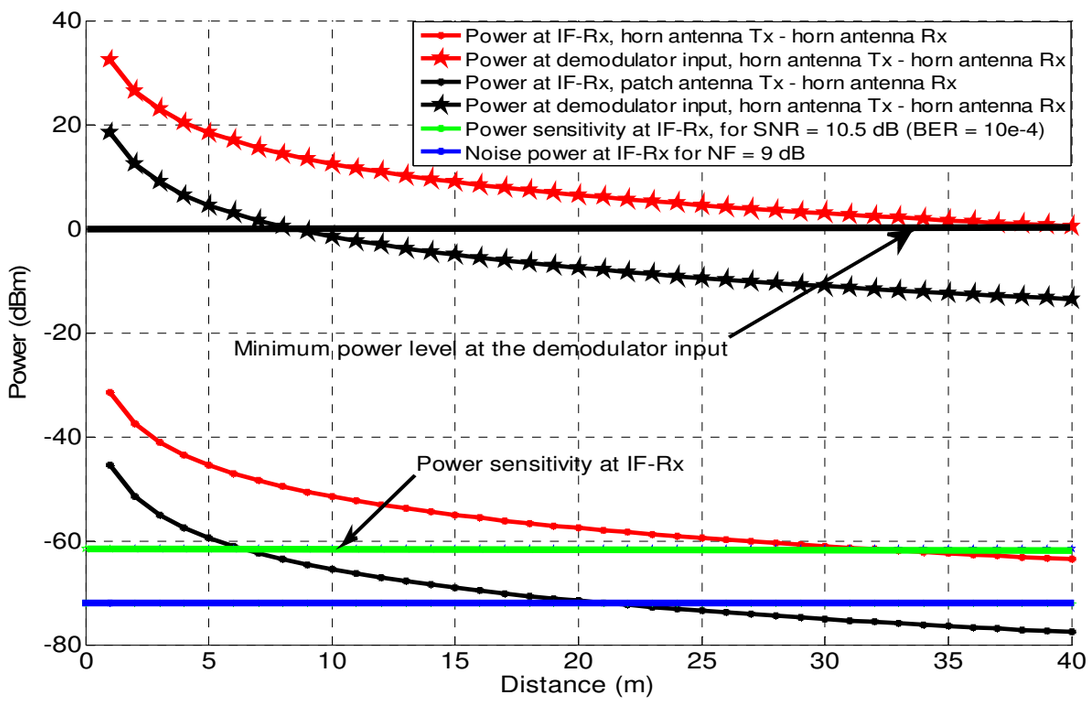

Fig. 21. The IF received power versus Tx-Rx distance

We can see that, a Tx-Rx distance of around 30 m can be achieved when using horn antennas at the transmitter and receiver, but only with 7 meters when using a patch antenna at Rx.

4.4 Indoor system performance

Based on the realized 60 GHz system, several measurements have been performed in a large gym and hallways, over distances ranging from 1 to 40 meters. At each distance, the BER was recorded during 5 minutes. The Tx and Rx horn antennas were situated at a height of 1.35 m above the floor. These measurements were conducted under LOS conditions with a fixed Rx and the Tx placed on a trolley pushed in a horizontal plane to various points about the environment. Also, during the measurements, the Tx and Rx were kept stationary, without movement of persons.

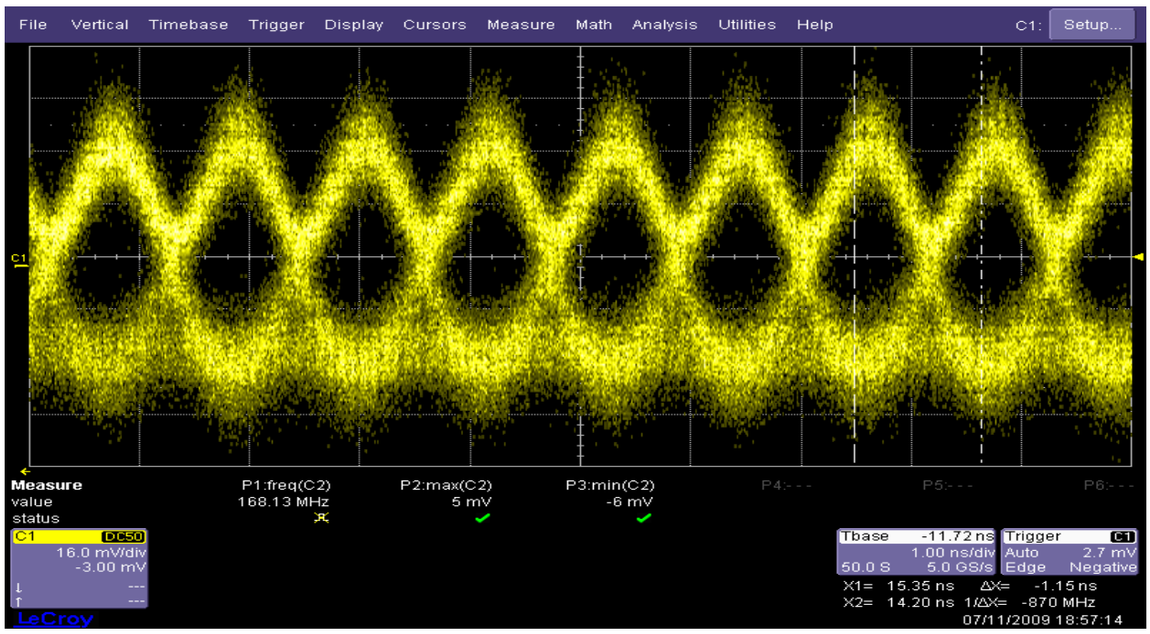

Fig. 22. Eye diagram for a 30 m Tx-Rx distance (in a large gym)

A pseudo-random sequence of 127 bits provided by a pattern generator was used as data source. Fig. 22 shows the eye diagram observed for a 30 m Tx-Rx distance (in a large gym). This suggests that a good communication link quality could be achieved at this distance.

We seek to evaluate the maximum distance attained between Tx-Rx for two possible configurations of an AGC amplifier, at minimum or maximum gain. Fig. 23 shows the measured BER results, with or without the AGC loop.

For a BER = 10^{-4}, when the amplifier gain is set at 8 dB, the upper limit of the Tx-Rx distance is about 7 m. However, the Tx-Rx distance can be increased at 35 m when the AGC gain amplifier is set at 28 dB.

As shown in Fig. 23, for the same BER = 10^{-6}, the Tx-Rx distance is around 27 m without channel coding and around 36 m with RS coding. This result proves the RS coding efficiency. Compared to the result in Fig. 21, a good agreement of a Tx-Rx maximum distance was obtained. This means that the multipath components are greatly reduced by the spatial filtering of the horn antennas (pencil beam).

However, the main problem of using directional antennas is the human obstruction. The signal reaching the Rx is randomly affected by people moving in the area and can lead to frequent outages of the radio link. For properly aligned antennas, it is confirmed that the communication is entirely interrupted when the direct path is blocked by a human body (synchronization loss). Therefore, an attenuation of around 20 dB was obtained when the direct path is blocked (as indicated in the power detector at the receiver). High gain antennas are needed for the 60 GHz radio propagation but to overcome this major problem, it is possible to exploit the angular diversity obtained by switching antennas or by beamforming (S. Kato et al., 2009). To improve the system reliability, a Tx mounted on the ceiling, preferably placed in the middle of the room can mitigate the radio beam blockage caused by people or furniture (S. Collonge et al., 2004). In real applications, the Tx antenna should have a large beamwidth to cover all the devices operating at 60 GHz in a room and the Rx antenna placed within the room should be directive so that the LOS components are amplified and the reflected components are attenuated by the antenna pattern.

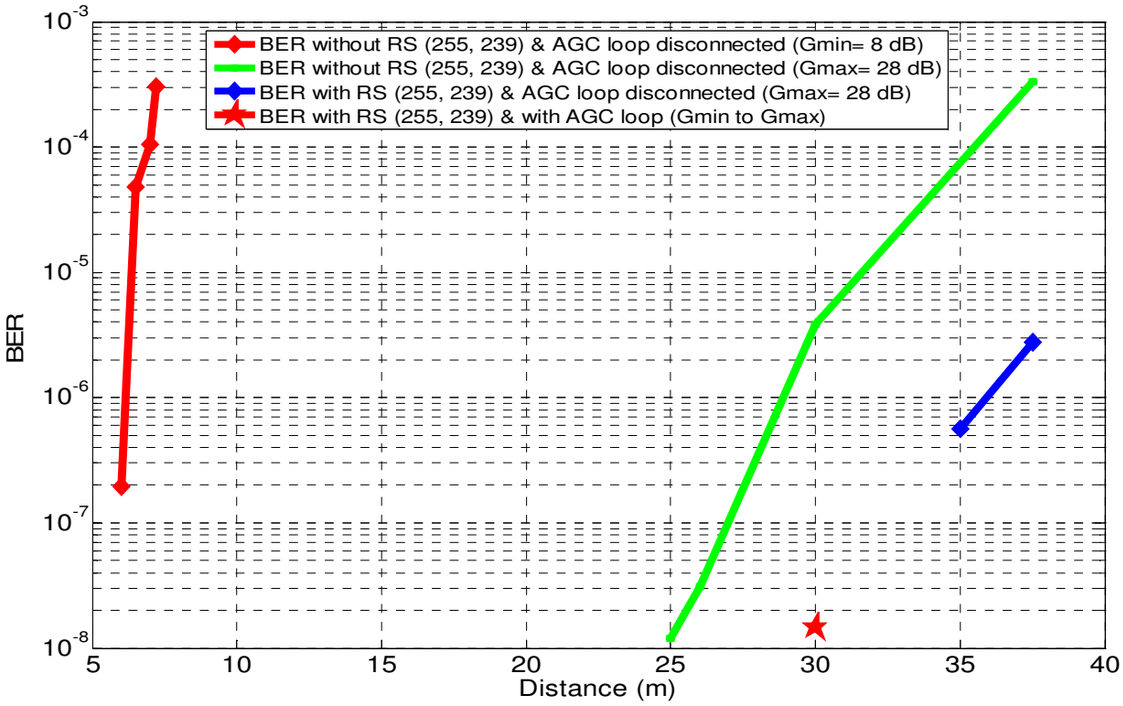

Fig. 23. BER versus the Tx-Rx distance in a large gym, using 32 bits preamble and S = 29

In order to examine the effects of the antenna directivity and the multipath fading, BER measurements were also conducted within a hallway over distances ranging from 1 to 40 meters. As shown in Fig. 24, the door of a 4 cm thickness (agglomerated wood), was opened during the BER measurements. The hallway has concrete walls and wooden doors on both sides. The Tx-Rx antennas (placed in the middle of the hallway) were positioned at a height of 1.35 m. The idea was to analyze the results of BER measurements with and without RS coding in a hallway separated by a door.

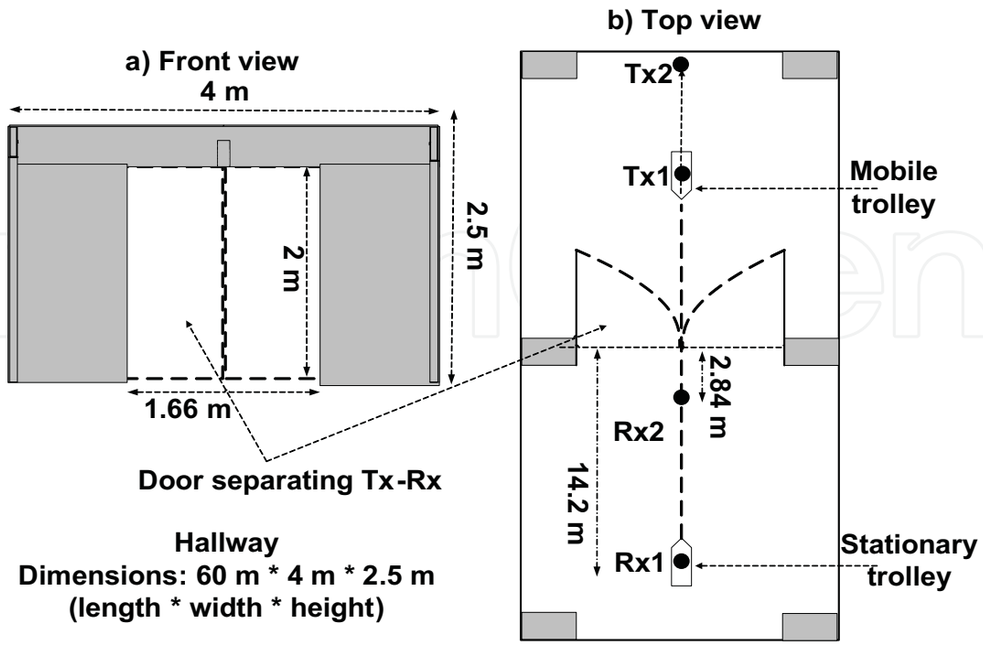

Fig. 24. The hallway: a) Front view; b) Top view

Due to the guided nature of the radio propagation along the hallway, the major part of the transmitted power is focused in the direction of the receiver. This means that in hallway the path loss exponent is considered less than 2 (as in a free space model). In the hallway, the door and walls can cause reflections and diffractions of the transmitted signal, in particular when the Rx position is far away from the opening door (as Rx1 position shown in Fig. 24). We found that for the same 32 m Tx-Rx distance, the received signal power was similar for both positions Tx1-Rx1 and Tx2-Rx2. However, the BER without coding is equal to $2.8*10^{-2}$ (due to some synchronization losses) and $2.8*10^{-5}$ for Tx1-Rx1 and Tx2-Rx2 positions, respectively. In the case of Tx1-Rx1 position, diffractions and reflections from the borders of the opening door can be the dominant contributors to the significant BER degradation.

BER measurements versus Tx-Rx distance using 64 bits preamble ($\gamma = 58$) were also carried out (in the case of Rx2 position). We found that for a Tx-Rx2 distance less than 32 m, all transmitted bits are received without errors (with RS coding) during 5 minutes measurement. Compared to the result obtained with the 32 bits preamble, as shown in Fig. 23, our investigation revealed that the frame structure using 64 bits preamble is better than 32 bits preamble in terms of byte/frame synchronization.

We also evaluate the BER performance when the door is closed. We observed that the attenuation increases of about 15 dB. A similar value was obtained in (S. Collonge et al., 2004). In this situation, the propagation channel is also unavailable during the "shadowing events" and lead to permanent synchronization loss. Therefore, radio electric openings (windows ...) are necessary.

We seek to determine also the BER degradation in function of Rx antenna depointing, as shown in Fig. 25. Measurement was done in a large gym and each BER result is recorded during 5 minutes. The distance between Tx-Rx is fixed but only the antenna Rx is slightly

turned at right or at left. We found that the synchronization loss can be obtained at a BER of around 10^{-4} which corresponds to the Rx beam depointing of around 12°. This means that the Rx horn antenna needs to be properly well aligned in the direction of the Tx beam antenna. In a hallway environment, the misalignment of beam antennas (of a few degrees) can seriously influence the BER performance due to the multipath components caused by the sides of walls and the door borders. In the worst case, the misalignment errors can lead to occasional synchronization losses, giving a BER higher than 10^{-4}.

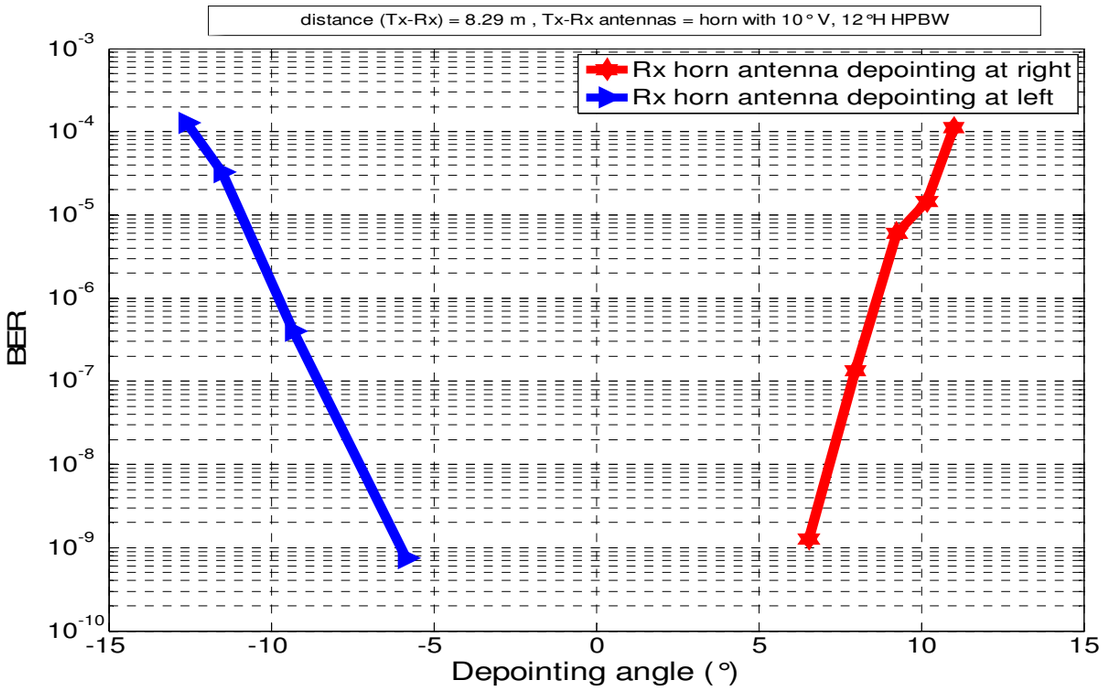

Fig. 25. BER as a function of an Rx antenna misalignment

5. Conclusion

In this chapter, a brief overview of several studies performed at IETR on 60 GHz indoor wireless communications is presented. The characterization of the radio propagation channel is based on several measurement campaigns realized with the channel sounder of IETR. Some typical residential environments were also simulated by ray tracing and Gaussian Beam Tracking. The obtained results show a good agreement with the experimental results. Recently, the IETR developed a single carrier wireless communication system operating at 60 GHz. The realized system provides a good trade-off between performance and complexity. An original method used for the byte/frame synchronization is also described. The numerical results show that the proposed 64 bits preamble allows obtaining better BER results comparing to the previously proposed 32 bits preamble. This new frame structure allows obtaining a high preamble detection probability and a very small false alarm probability. As a result, a Tx-Rx distance greater than 30 meters was attained with low BER using high gain horn antennas. In order to support a Gbps reliable transmission within a large room and severe multipath dispersion, a convenient solution is

to use high gain antennas. However, our investigation revealed that the high gain antenna directivity stresses the importance of the antennas pointing precision. In addition, the use of directional antennas for 60 GHz WPAN applications is very sensitive to objects blocking the LOS path. Due to the hardware constraints, the first data rate was chosen at 875 Mbps. Using a new CDR circuit limited at 2.7 Gbps, a data rate of 1.75 Gbps can be achieved with the same DBPSK architecture or with DQPSK architecture. For suitable quality requirements in Gbps throughput, an adaptive equalizer should be added to counteract the ISI influence. The demonstrator will be further enhanced to prove the feasibility of wireless communications at data rates of several Gbps in different environments, especially in non line-of-sight (NLOS) configurations.

6. References

ECMA (2008) . Rate 60 GHz PHY, MAC and HDMI PAL, Standard ECMA-387, December 2008. *[online]: http : // www.ecma-international.org /publications /standards /Ecma-387.htm*.

P. F. M. Smulders (2002). Exploiting the 60 GHz Band for Local Wireless Multimedia Access: Prospects and Future Directions, *IEEE Communications Magazine*, Vol. 40, No. 1: 140-147.

C. C. Chong, K. Hamaguchi, P. F. M. Smulders and S. K. Yong (2007). Millimeter-Wave Wireless Communication Systems: Theory and Applications, *EURASIP Journal on Wireless Communications and Networking*, Vol. 2007, article ID 72831, 89 pages.

G. El Zein (2009). Propagation Channel Modeling for Emerging Wireless Communication Systems, *IEEE ACTEA 2009*: 457 – 462, Zouk Mosbeh, Lebanon.

S. Guillouard, G. El Zein and J. Citerne (1999). Wideband Propagation Measurements and Doppler Analysis for the 60 GHz Indoor Channel. *in Proc. IEEE MTT-S International Microwave Symposium* , 1751-1754, Anaheim - CA, USA.

S. Collonge, G. Zaharia and G. EL Zein (2004). Influence of Human Acitivity on Wideband Characteristics of the 60 GHz Indoor Radio Channel, *IEEE Transactions on Wireless Communications*, Vol. 3, No. 6: 2396-2406.

P. F. M. Smulders (2009). Statistical Characterization of 60 GHz Indoor Radio Channels, *IEEE Transactions on Antennas and Propagation*, Vol. 57, No. 10 (October 2009): 2820-2829.

N. Moraitis and P. Constantinou (2004). Indoor Channel Measurements and Characterization at 60 GHz for Wireless Local Area Network Applications, *IEEE Transactions on Antennas and Propagation*, Vol. 52, No. 12: 3180–3189.

R. Tahri, D. Fournier, S. Collonge, G. Zaharia and G. El Zein (2005). Efficient and fast gaussian beam-tracking approach for indoor-propagation modeling, *Microwave and Optical Technology Letters*, Vol. 45, No. 5: 378-381.

S. Kato, H. Harada, R. Funada, T. Baykas, C. Sean Sum, J. Wang and M. A. Rahman (2009). Single Carrier Transmission for Multi-Gigabit 60-GHz WPAN Systems, *IEEE Journal on Selected Areas in Communications*, vol. 27, No. 8: 1466-1478, ISSN: 0733-8716.

L. Rakotondrainibe, Y. Kokar, G. Zaharia, G. Grunfelder and G. EL Zein (2009). Toward a Gigabit Wireless Communications System, *International Journal of Communication Networks and Information Security (IJCNIS)*, Vol. 1, No. 2: 36-42.

K. C. Huang and D. J. Edwards (2008). Millimeter Wave Antennas for Gigabit Wireless Communications: A Practical Guide to Design and Analysis in a System Context, in *book chapter, a John Wiley and Sons Ltd,* 291 pages, ISBN 978-0-470-51598-3 (HB).

U. H. Rizvi, G. J. M. Janssen and J. H. Weber (2008). Impact of RF Circuit Imperfections on Multi-carrier and Single-carrier based Transmissions at 60 GHz, *in Proc. IEEE Radio and Wireless Symposium*, 691–694, ISBN: 978-1-4244-1463-5.

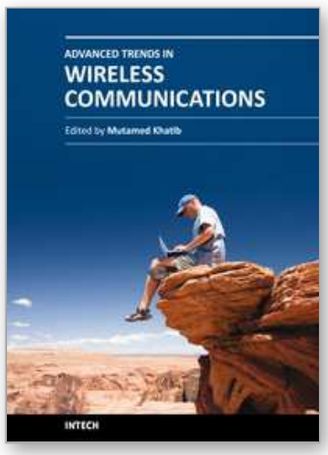

Advanced Trends in Wireless Communications

Edited by Dr. Mutamed Khatib

ISBN 978-953-307-183-1
Hard cover, 520 pages
Publisher InTech
Published online 17, February, 2011
Published in print edition February, 2011

Physical limitations on wireless communication channels impose huge challenges to reliable communication. Bandwidth limitations, propagation loss, noise and interference make the wireless channel a narrow pipe that does not readily accommodate rapid flow of data. Thus, researches aim to design systems that are suitable to operate in such channels, in order to have high performance quality of service. Also, the mobility of the communication systems requires further investigations to reduce the complexity and the power consumption of the receiver. This book aims to provide highlights of the current research in the field of wireless communications. The subjects discussed are very valuable to communication researchers rather than researchers in the wireless related areas. The book chapters cover a wide range of wireless communication topics.

How to reference

In order to correctly reference this scholarly work, feel free to copy and paste the following:

Ghaïs El Zein, Gheorghe Zaharia, Lahatra Rakotondrainibe and Yvan Kokar (2011). Indoor Channel Characterization and Performance Analysis of a 60 GHz near Gigabit System for WPAN Applications, Advanced Trends in Wireless Communications, Dr. Mutamed Khatib (Ed.), ISBN: 978-953-307-183-1, InTech, Available from: http://www.intechopen.com/books/advanced-trends-in-wireless-communications/indoor-channel-characterization-and-performance-analysis-of-a-60-ghz-near-gigabit-system-for-wpan-ap

INTECH
open science | open minds

InTech Europe
University Campus STeP Ri
Slavka Krautzeka 83/A
51000 Rijeka, Croatia
Phone: +385 (51) 770 447
Fax: +385 (51) 686 166
www.intechopen.com

InTech China
Unit 405, Office Block, Hotel Equatorial Shanghai
No.65, Yan An Road (West), Shanghai, 200040, China
中国上海市延安西路65号上海国际贵都大饭店办公楼405单元
Phone: +86-21-62489820
Fax: +86-21-62489821

IntechOpen